N E Zhukovsky Central Aero-Hydrodynamics Institute (TsAGI)
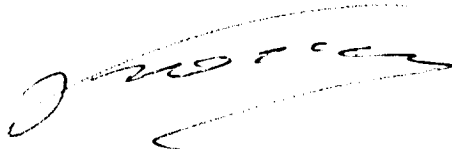
Final report of TsAGI under cooperative agrement # NCCW-72

Receptivity of Flat-Plate Boundary Layer in a Non-Uniform Free Stream (Vorticity Normal to the Plate)

Chief of Project   Kogan M.N.

1. Introduction

Recent progress in both the linear and nonlinear aspects of stability theory has highlighted the importance of receptivity problem [1]. One of the most unclear part of receptivity studies is the receptivity of boundary-layer flow to vortical disturbances. Some experimental [2] and theoretical [3] results permits to propose that quasi-steady outer-flow vortical disturbances may trigger by-pass transition. For this reason the experimental and theoretical study of vortex-boundary layer interaction is an actual task. In present work such interaction is investigated for the vorticity normal to the leading edge. The interest to this type of vortical disturbances arises from the theoretical work [4], where it was shown that small sinusoidal variation of upstream velocity along the spanwise direction can produce significant variations in the boundary-layer profile.

In experimental part of this work such non-uniform flow was created and laminar-turbulent transition in this flow was investigated. The non-uniform flow was produced by laminar or turbulent wake behind the wire placed normal to the plate upstream the leading edge. Theoretical part of the work is devoted to studying the unstable disturbance evolution in a boundary layer with strongly non-uniform velocity profile similar to that produced by outer-flow vorticity.

2. Experimental study of wake-boundary layer interaction

2.1. Experimental setup and equipment

The experiment was carried out in a low-turbulence direct-flow wind tunnel T-36I (see Figure 1) of Central Aerohydrodynamic Institute (TsAGI). The test section is 2610 mm long, 500 mm wide and 350 mm high. The left and right walls were adjusted to compensate for boundary-layer growth and to obtain a zero streamwise pressure gradient. A variable-speed motor and a motor controller drives an axial flow fan. The free-stream velocity was monitored using a Pitot tube. The wind tunnel was designed for velocity range of $15 \div 65$ m/s, but fan supply the lower velocities from 2 m/s. The input nozzle has exit to throat area ratio 11.62. Before the nozzle a set of 4 deturbulence nets were placed. All nets were made from 0.12 mm wires and have square mesh 0.3 × 0.3 mm.

Laminar-turbulent transition was studied in the boundary layer at horizontally mounted flat plate of 1810 mm long, 500 mm wide and 15 mm thick. The plate was made of Plexiglass and has semi-elliptical nose with 18:1 axis ratio. The high from bottom wall to plate was 125 mm, the distance from beginning of test section to leading edge was 710 mm. To produce the local flow inhomogeneity the metal wire of 0.1, 0.8 or 1.6 mm was stretched vertically in special support at different distances before leading edge of plate.

The streamwise velocity component was measured with a DISA 55M01 anemometer and a single hot wire probe Dantec 55P01 or 55P15 made of gold plated tungsten with a wire diameter 5 μm and a sensitive length of 1 mm. Signals from hot-wire anemometers were filtered to reduce noise level, digitized by 12-bit A/D converter (National Instruments AT-MIO-64-E-3) and processed on a computer. The low-pass filter cutoff frequency was 1 kHz at 36 dB/octave. The high-pass filter cutoff frequency was 5 Hz at 36 dB/octave. Mean flow velocity was measured without filters. The sampling frequency was 5 kHz . Realization of 100 s long was used for spectrum calculation and 20 s long realizations

were used for mean velocity and pulsations determining.

2.2. Undisturbed flow characteristics

For the wake-boundary layer interaction study the wind tunnel was re-adjusted to obtain low turbulent flow at small speeds of $5 \div 10$ m/s. Detailed measurements of mean velocity field and pulsations at these speeds were made. The mean velocity field inhomogeneity in the test section was found to be about 0.5 % of u_∞. Characteristics of pulsations are given in table 1. Despite of all attempts to diminish the turbulence level, the integral pulsations at the small speeds remain high enough. However, the most part of pulsation energy is accounted for the extremely low-frequency pulsations. This fact is illustrated by spectrum of velocity pulsation for speed 5 m/s shown in Figure 2. If signal was filtered by high-pass filter with cut of point at 5 Hz, the pulsation level becomes an order low (see table 1). Frequencies less then 5 Hz correspond to characteristic sizes greater then 1 m. Really, the pulsations of these frequencies are caused by temporal drift of velocity in the wind tunnel and have no relation to turbulence. So, the filtered pulsations will be used further as the characteristic of turbulence level.

2.3. Flow in the wake behind the wire

Laminar and turbulent wakes with different velocity deficits and width were created and mean velocity profile and pulsations in the wakes were measured. Flow configuration and coordinate system used in this case is shown in Figure 3a. In order to increase the accuracy of mean velocity profile measurement in low-deficit wake, the measurements were made by two probes. The first probe was placed into the wake, the second probe was placed into free stream. The difference between the velocities measured by these probes was velocity deficit in the wake. Usage of two probes eliminates the errors caused by velocity drift and variations of temperature. The accuracy of mean velocity measurements by two-probe method is about 0.3 %, whereas if only one probe is used the error increases to 0.8 %.

The laminar wake was produced by 0.1 mm wire placed in flow with speed 5 m/s. The Reynolds number corresponding to flow over wire was $R_D = u_\infty D/\nu = 34.5$, which is less then critical value $R_* \sim 40$ for steady flow over cylinder. Mean velocity profiles measured at distances $x/D = 100, 360, 1060$ from the wire are shown at Figure 4. Theoretical expression for the velocity profile in laminar wake is

$$\overline{u} = c^{-\ln 2\eta^2} \quad , \quad \overline{u} = \frac{u - u_\infty}{u_0} \quad , \quad \eta = \frac{z}{L} \tag{2.1}$$

where velocity deficit u_0 and half-thickness of the wake L are given by

$$\frac{L}{D} = A\sqrt{\frac{x}{D}} \ , \quad \frac{u_0}{u_\infty} = B\sqrt{\frac{D}{x}} \ , \quad A = 2\sqrt{\frac{\ln 2}{R_D}} \ , \quad B = \frac{C_x}{4}\sqrt{\frac{R_D}{\pi}} \tag{2.2}$$

Velocity profiles plotted in similarity coordinates $\overline{u}$, η in Figure 5a collapse quite neatly onto a curve described by (2.1) . The graphs of L/D and $\overline{u}$ as functions of $\sqrt{x/D}$ and $\sqrt{D/x}$ are shown in figure 5 b and c respectively. They are linear in accordance with (2.2). Slope coefficient $A = 0.28$ found from Figure 5b well coincides with theoretical value $A = 0.283$.

2

Unfiltered velocity pulsations and filtered pulsations for $f > 5$ Hz are shown in Figures 6a and 6b. Filtered pulsations are almost equal to their value in the free stream. So the increase of unfiltered pulsation level at sides of wake is caused by low frequency oscillations and may be treated as quasi-steady displacement of wake in z-direction. The data obtained permit us to conclude that the wake behind 0.1 mm wire is do laminar.

To produce the turbulent wake the wire of 1.6 mm diameter was placed in flow with velocity 10 m/s. The Reynolds number corresponding to flow over wire was $R_0 = 1100$, which is large enough for developed turbulent wake production. The profiles of mean velocity and pulsations measured at distance x/D =220 are shown in Figure 7. Due to pulsation level is high enough, the filtered pulsations for $f > 5$ Hz highly differs from unfiltered pulsations. The shape of pulsations profile with two maxima found here is familiar for small deficit turbulent wake. From the shape of mean velocity profile the velocity deficit $u_0 = 0.0633\ u_\infty$ and half-thickness of the wake $L = 4.0D$ were found. These values found from universal laws [5] with constants from the experiment [6] $u_0 = 0.0647\ u_\infty$, $L = 3.88D$ are in good agreement with data of our measurements.

The spectra of velocity pulsations measured at the centerline of the wake and at the boundary of it ($z/L = 2.5$) are presented in Figures 8a and 8b. The irregular behavior of the spectrum at the boundary of the wake for $f < 100$ Hz is caused by the relatively high low-frequency pulsations in the wind-tunnel flow. In the same graphics the points showing the generalization of the spectra measured in the flat-plate wake [6] are plotted. In the centerline the agreement of our data and [6] is excellent. Rather poor agreement of spectrum at the boundary of the wake with [6] may be caused by different distance from the wake center in our and [6] measurements (in [6] the spectrum at the boundary was measured for $z/L = 3$). Generally, the data presented here shows that the turbulent wake in our wind tunnel has the same parameters as the turbulent wake in the good low-turbulent wind tunnels.

2.4. Interaction of wake with flat-plate boundary layer

In this section preliminary results on wake-boundary layer interaction are reported. All mean-flow profiles presented in this section were measured by one probe, so the accuracy of these measurements is about 1% of outer flow velocity. In future the accuracy of mean-flow measurements may be enhanced by means of two-probe method adaptation to boundary-layer flow conditions.

Flow configuration and coordinate system used in this section are shown in Figure 3b. The wake produced by vertically stretched wire interacts with boundary layer over the horizontally mounted plate. For preliminary studies reported here the plate with semi-elliptical nose with 18:1 axis ratio was used. In subsequent more detailed investigation the plate with expendable noses with different axis ratios (8:1, 4:1 etc.) will be used. Plate was mounted at zero angle of attack so zero pressure gradient at the upper plate surface occurs. The static pressure nonuniformity along the plate surface was less then 1%. Due to sufficiently large low-frequency pulsations in the wind tunnel, special efforts were made to ensure that there are no local (in time) flow separations from leading edge.

At first effect of laminar wake behind 0.1 mm wire at 5 m/s speed on boundary layer was studied. The distortion of mean flow in boundary layer at $x = 200$ mm from leading edge was found to be within the experimental error, even for minimal distance from wire

3

to leading edge $x_0 = 40$ mm. No distinct maximum in velocity pulsation's distribution over the span was found yet. So, the influence of laminar wake on boundary-layer flow is weak enough, instead of sufficiently large velocity deficit of the wake $u_0/u_\infty \approx 6\%$ when it meets the leading edge of the plate. Possible explanations of this phenomenon see in Section "Discussion".

All positive results obtained here deals with turbulent wake action on boundary layer transition. These measurements were done at velocity 10 m/s. All diameters and positions of wire used and characteristics of wakes generated at the plate's nose location are listed in Table 2. Streamwise dependencies of mean flow velocity and pulsations ($f > 5$ Hz) in boundary layer exactly behind the wire ($z = 0$) for all these configurations are shown in Figure 9. These data correspond to fixed $y = 0.5$ mm. Figure 9 demonstrates that turbulent wake strongly affects on transition. If no wire is installed, the transition does not occur up to the end of plate. By means of choosing the wake parameters the place of transition may be moved from the near nose to the end of plate.

Amplification curves of pulsations measured for wake-boundary layer interaction are similar to these for boundary layer transition in flow with enhanced turbulence level [7]. At least for sufficiently weak wakes (I and II in Table 2), two stages of transition process may be distinguished. At the first stage the pulsations in boundary layer are nearly constant and seems be proportional to pulsations in the wake. The second stage is characterized by fast growth of pulsations.

More detailed study of flow field was done in the configuration III from Table 2. In sections $x = 200$, 350, 525, 670, 850 mm the profiles of mean velocity and filtered pulsations ($f > 5$ Hz) were measured in the boundary layer and at the outer edge of it. These profiles are shown in Figure 10. Profiles in boundary layer were measured at different distances from the wall, which are found from condition $u = 0.5u_\infty$. Outer flow profiles correspond to fixed $y = 7$ mm.

Figure 10 clearly demonstrate that both mean flow distortion and pulsations amplify in boundary layer. The character of this amplification is qualitatively different before and after growth of disturbances. In sections $x = 200$ mm and $x = 350$ mm before the growth the shape of pulsations profile in boundary layer is similar to that in outer flow. The shape of streamwise distribution of mean velocity sufficiently differs from these distribution in the outer flow, but the width of disturbed domain in boundary layer is the same that in the outer flow. After rapid growth of disturbances (sections $x = 670$ mm and $x = 850$ mm) the pulsations and the mean flow distortion in the boundary layer spreads in spanwise direction. Shape of pulsation profile here sufficiently differs from distributions of pulsations in the outer flow.

Vertical profiles of mean velocity and filtered pulsations in the centre of the wake at the same sections are shown at the Figures 11a and 11b. In two first sections $x = 200$ mm and $x = 350$ mm the mean velocity profiles are close to that in Blasius boundary layer plotted by thick solid line in Figure 11a. Profiles in two last sections ($x = 670$ mm and $x = 850$ mm) are close to each other and are similar to turbulent boundary layer profile. Shapes of pulsations profiles measured here are similar to analogues profiles obtained in experiments on transition in flow with enhanced turbulence level [7].

In addition to mean-flow velocity and pulsation distributions, spectra of velocity pulsations in the boundary layer and in the outer flow were measured at the same x-sections. These spectra $u_f(f)$ measured at the centerline ($z = 0$) and normalized such

4

that $\int_0^\infty u_f df = 1$ and $\int_0^\infty u_f df = u'$ are shown in Figure 12a and 12b. Normalization used in Figure 12a is convenient for study of evolution of spectrum shape whereas Figure 12b shows the relative amplitudes of pulsations of different frequencies. At the initial stage of transition the low-frequency pulsations predominantly grow. The most amplitude of these disturbances is reached just before the maximum of u' at $x = 525$ mm (see Figure 12b). At the later stage of transition at $x = 670$ mm and $x = 850$ mm the back energy flux from low to high frequencies occurs. Such evolution of spectrum is familiar for the transition in high turbulence level outer flow [7]. The spectra measured in the boundary of the wake within the boundary layer were almost the same as those at the centerline.

In spite of many attempts made, no phenomena which may be treated as TS waves were observed. So the mechanism of this transition should be assigned to by-pass one.

2.5. Discussion

The discrepancy between the above experimental results and predictions of Goldstain's work [4] is obvious. The results of [4] are based on "rapid distortion" theory [8] neglecting the viscous terms outside the boundary layer. This theory is valid if the length on which outer flow non-uniformity is deformed by flow inhomogeneity generated by nose is small with respect to characteristic length of viscous deformation. The last length L_v is connected with the spanwise size of distortion L by

$$L_v \sim \frac{u_0}{\nu} L^2$$

where for turbulent wake ν should be substituted by turbulent viscosity coefficient ν_T. It's easy to see that for distortion generated by wake, L_v is approximately equals to the distance from the wire to leading edge x_0. So the "rapid distortion" theory is valid if the length of deformation $x \ll x_0$. This condition was never fulfilled in our experiment, especially when laminar wake-boundary layer interaction was studied. In this case, on the contrary, $x \gg x_0$, and viscous forces are dominant. This is the reason of small impact of laminar wake on boundary-layer flow. For turbulent wake-boundary layer interaction $x \simeq x_0$, so the amplification of vortical disturbances by the flow deformation over the nose was partially damped by viscous forces.

Thus, to increase the wake action on boundary layer, the flow deformation produced by leading edge should be enhanced. This may be achieved by means of choosing more blunt leading edge.

When turbulent wake acts on boundary layer, the laminar-turbulent transition is caused by two factors: the turbulent pulsations in the wake and mean flow distortion. Unfortunately, the data obtained give no way for determining the relative roles of these factors. It is difficult to do in principle, because of pulsations in turbulent wake are proportional to velocity deficit. To distinguish the effect of mean flow distortion the experiment on wake-boundary layer interaction in the outer flow with enhanced turbulence level should be made. The radical way to separate the role of mean-flow distortion is to obtain the effect of laminar wake on transition. This effect may be enhanced using model with more blunt nose.

5

3. Interaction of Tollmien-Schlichting wave with steady flow inhomogeneity

In this section the Tollmien-Schlichting wave development in the boundary layer flow with spanwise variations of velocity profile is investigated. It's well known that such quasi-steady velocity variations generated by outer flow vortical disturbances play significant role in transition process. For this reason the influence of steady inhomogeneity of flow on boundary layer stability is an actual problem studied in large amount of works. Most of them [9, 10] are made in the frame of different asymptotic schemes valid for $R \to \infty$ and small amplitude of disturbances. So the results of [9, 10] are not suitable for real experimental conditions where Reynolds number is finite and amplitude of flow inhomogeneity is sufficiently large.

In this section the Tollmien-Schlichting wave and steady disturbances interaction is studied for finite R and amplitude of disturbances. The study is based on calculation of spatial evolution of disturbances by parabolic stability equations (PSE) method.

3.1. Numerical method

Consider the flow of incompressible viscous fluid over an infinite flat plate. Let be x -the streamwise direction, y -the direction normal to wall and z -the spanwise direction. The lengths and velocities are written in non dimensional form using the upstream velocity u_∞ and a constant length $\delta = (\nu \tilde{x}_0 / u_\infty)^{\frac{1}{2}}$ (boundary layer thickness at the dimensional distance $\tilde{x}_0$ from leading edge). The velocity vector $\mathbf{V}$ is decomposed into the two-dimensional basic flow $\mathbf{V_0}$ corresponding to Blasius boundary layer and finite- amplitude three-dimensional disturbance $\mathbf{V_p}$ as

$$\mathbf{V}(x, y, z, t) = \mathbf{V_0}(x, y) + \mathbf{V_p}(x, y, z, t) \tag{3.1}$$

A disturbance is assumed to be periodic in t and z and is written as

$$\mathbf{V}_p = \sum_{n=-N}^{N} \sum_{m=0}^{M} \left(\mathbf{V}_{mn}(x, y) e^{im(\alpha(x) - \omega t) + in\beta z} + c.c \right) \tag{3.2}$$

Here the amplitudes $\mathbf{V}_{mn}$ and longitudinal wavenumber are assumed to be slowly changing functions of x, such that terms like $\partial^2 \mathbf{V}_{mn}/\partial x^2$, $\partial^2 \alpha/\partial x^2$ can be neglected. With these assumption, the substitution of (3.1),(3.2) into Navier-Stokes equations, yields a set of partial differential equations of parabolic type

$$\hat{\mathbf{L}}_{mn}^1 \frac{\partial \mathbf{V}_{mn}}{\partial x} + \hat{\mathbf{L}}_{mn}^2 \mathbf{V}_{mn} + \hat{\mathbf{L}}_{mn}^3 \frac{\partial \alpha}{\partial x} \mathbf{V}_{mn} = \mathbf{N}_{mn}(\mathbf{V}_p) \tag{3.3}$$

with boundary conditions

$$\mathbf{V}_{mn}(0) = \mathbf{V}_{mn}(\infty) = 0$$

and initial conditions in some section $x = x_0$

$$\mathbf{V}_{mn}(x_0, y) = \mathbf{F}_{mn}(y) \quad \alpha(x_0) = \alpha_0$$

6

Here $\hat{L}^1_{mn}, \hat{L}^2_{mn}, \hat{L}^3_{mn}$ are linear operators including derivatives in y, N_{mn} represents the nonlinear terms. Details of derivations of parabolic stability equations (3.3) and expressions for $\hat{L}^1_{mn}, \hat{L}^2_{mn}, \hat{L}^3_{mn}$ see in [11, 12].

The set of equations (3.3) was solved by a marching procedure in x. For approximation of it in x the implicit finite difference scheme was used with iterations employed for nonlinear terms evaluations. The spectral collocation method was used for discretization of (3.3) in y. In distinction to [11] no normalization conditions for amplitude functions V_{mn} was introduced, and $\alpha(x)$ dependence was found from condition of minimal change of $\arg(V_{mn})$ over each step.

To test the numerical method described here and code for it's realization we repeated the calculations of non-linear evolution of two-dimensional TS wave made in [11]. The initial conditions were set at $R_0 = \delta u_\infty/\nu = 400$, the reduced TS wave frequency was $F = \omega\nu/u_\infty^2 = 8.6 \times 10^{-6}$. Six Fourier components in (3.2) were used, with frequencies $0F, 1F, ..., 5F$. The variation of u'_{max} with the Reynolds number obtained by our code and in [11] are shown by solid and dashed lines in figure 13. The upper lines 1 and 2 are the amplitudes of TS wave for 0.25% and 0.3% initial amplitude level, the lower lines 1 and 2 are the amplitudes of the second harmonics for the same initial amplitudes. Good coincidence of our results and [11] demonstrates high accuracy of code developed.

Another test made was modeling of three-dimensional disturbances evolution in the experiment on subharmonic transition [13]. Figure 14 represents the amplitude of primary TS wave (solid line) and subharmonic (dashed line). Points shows experimental data of [13]. The results of PSE-method are in good agreement with experiment.

3.2. Results

For study of interaction of TS wave with steady flow inhomogeneity, the initial conditions with non zero harmonics 10 and $0n$, $n = 1, ..., N$ were used. The harmonic 10 corresponds to plane TS wave, the $0n$ harmonics describe the steady flow velocity variation in spanwise direction. From our point of view, the most interesting is the flow inhomogeneity localized in narrow stripe. Such steady flow distortion may be produced by the suction or blowing of fluid throw the wall which is distributed in accordance with following expression

$$w(x, 0, z) = \epsilon(1 - q) \exp\left(-\frac{(x - x_c)^2}{\Delta^2}\right) \sum_{n=1}^{N} q^{n-1} \cos n\beta z$$

where ϵ is amplitude, x_c -center, Δ - characteristic length of suction or blowing distribution. If $q = 1 - \kappa$, $\kappa \ll 1$, then distribution of suction in spanwise direction has narrow maximum at $z = 0$. For small amplitude of suction ϵ the steady flow distortion behind the suction area may be found in the frame of parallel flow assumption by receptivity theory method developed in [14]. Such flow at large enough distance from suction domain was used as an initial condition for harmonics $0n$, $n = 1, ..., N$. Specifically, the flow produced at initial section $x = x_0 = R_0 = 800$ by suction or blowing distribution with $\beta = 0.02$, $q = 0.95$, $x_c = 600$, $\Delta = 20$, $N = 40$ and different ϵ was used as an initial conditions for steady flow distortion. The maximum of steady velocity distortion in the initial section Δu_{0m} will be used further as a characteristic of steady flow inhomogeneity instead of suction amplitude ϵ.

7

Steady flow inhomogeneity generated in initial section is shown in figure 15, with figure 15 a shows spanwise distribution of flow distortion at $y = 2.64$ (normalized by it's maximum) and figure 15 b demonstrates the velocity profiles for $z = 0$ and different Δu_{0m}.

The influence of different amplitude steady flow distortions on the development of plane TS wave with $\omega = 0.032$ and amplitude $u'_{max} = 10^{-3}$ was studied. This TS wave was used as an initial condition for harmonic 10. The number of harmonics in expression for velocity (3.2) was $M = 4$, $N = 40$. Evolution of TS wave in flow with $\Delta u_{0m} = \pm 0.01, \pm 0.1, \pm 0.2, \pm 0.3$ was computed. Because of PSE-method does not works at later stage of transition, the computations were stopped when the amplitude of velocity pulsations reached 0.1 in any point of (y, z) plate. The streamwise coordinate x_* where this occurs is treated as an approximate place of laminar-turbulent transition. In figure 16 the transition location x_* as function of Δu_{0m} is shown, with solid and dashed lines shows results for negative and positive Δu_{0m}.

The amplitudes of pulsations for fixed $y = 2.64$ as functions of Reynolds number for negative and positive Δu_{0m} are plotted in figures 17 a and b. Maximal over z amplitudes are shown by dashed lines, whereas solid lines correspond to pulsations in "undisturbed" flow between the maximums of steady flow distortion ($z = \pm \pi / \beta$). Results for $\Delta u_{0m} = \pm 0.01, \pm 0.1, \pm 0.2, \pm 0.3$ are designated by figures $1, 2, 3, 4$, respectively. Comparison of figures 17 a and b reveals qualitative different character of disturbances growth for steady flow inhomogeneities with positive and negative Δu_{0m}. For positive Δu_{0m} maximal pulsations slightly exceed the pulsations in the "undisturbed" flow and steady inhomogeneity highly affects on transition process. In contrast, for negative Δu_{0m} the maximal pulsations are in order of magnitude grater then the pulsations in the "undisturbed" flow. The maximums of pulsations in this case are located within the regions of velocity deficit. This may be explained by two causes. The first one is the inflexible instability of velocity profile at the region of velocity deficit. For $\Delta u_{0m} \leq -0.1$ the inflection point do exists in the initial velocity profiles at $z = 0$ (see figure 15 b), but it disappears during evolution of steady disturbances. The places where these points disappear are shown by arrows in figure 17 a. Nevertheless, after the inflection point dies out, the character of disturbances evolution does not qualitatively changes. Consequently, another mechanism should be responsible for pulsations growth in velocity deficit regions. This mechanism may be explained in the following manner. The phase velocity of TS wave in the velocity deficit region is less then this in the undisturbed flow. In accordance with the laws of geometrical optics, the beams are concentrated in the regions of lesser phase velocity. Analogous effect, seams to be the reason of pulsations growth in the velocity deficit regions.

At later stages of transition pulsations reached large amplitude and triggered the deformation of the shape of steady flow distortion. This effect is illustrated by figure 18, where spanwise distribution of mean flow velocity and pulsations near transition are shown. These data corresponds to initial maximum flow distortion $\Delta u_{0m} = -0.1$. It is interesting to note, that the shapes of mean velocity and pulsations distributions are qualitatively similar to those measured in experiment on wake-boundary layer interaction (see figure 10).

It should be mentioned that TS wave - mean flow inhomogeneity interaction modelled here not directly concerns the wake-boundary layer interaction studied in section 2. Nevertheless, instead of different nature of velocity pulsations some mechanisms of disturbances evolution may be the same.

4. Passage of instability wave over strong surface irregularity

The suppression of instability waves in boundary-layer flow is of fundamental importance in connection with the problem of laminar-turbulent transition delay. There exist two main types of methods using to suppress TS waves. The first type includes various kinds of distributed control for stabilization the mean flow. The compliant wall used to reduce the growth rates of instability waves is the classical example of such a method [15](Kramer, 1957). The second type of methods, first offered by Milling [16], applies the principle of unstable wave cancellation by means of the formation of artificial instability wave with the same frequency and amplitude but opposite phase.

In this paper we investigate the suppression of unstable oscillations based on the interaction between TS wave and longitudinal irregularity caused by 2D compliant strip on a rigid wall. Finite Reynolds number approach is used for theoretical and numerical analysis. The results obtained admit equivalent physical interpretations within the framework of methods of both the above-mentioned types: quantitative TS wave attenuation characteristics can be obtained both by studying the stabilizing effect of the wall flexibility and by analyzing the formation of the secondary TS wave generated by the vibration of the compliant part of the wall. This connection between stability and receptivity phenomena have been pointed out in [17] for the problem of TS wave passage through a channel with a local change of wall geometry.

Here we also study the interaction between boundary-layer inhomogeneity and eigenmodes of other types (discrete or continuous). The quantitative characteristics of eigenmode modification - passage coefficient, transformation coefficient and transmutation coefficient - are introduced. The results of the investigation show the equivalence of stability and receptivity phenomena in inhomogeneous boundary layer.

Note that the generation of artificial disturbances by a vibrator in boundary layer on a wall with 2D elastic section has been investigated by Terent'ev [18] using the assumptions of triple-deck theory. The problem of TS wave propagation over the join between a rigid and compliant channel wall has been examined by Davies & Carpenter [19] using direct numerical simulation.

4.1. Stability of boundary-layer flow on a wall of uniform flexibility

Let us consider a compressible boundary layer on a flat plate. We introduce a coordinate system, with the origin at some point on the plate surface, with a streamwise x-axis, and with a y-axis normal to the wall. The system of units is the same as in [14]. All numerical examples are cited for Mach number $M = 0.8$, Prandtl number $\mathrm{Pr} = 0.75$, and specific heat ratio $\kappa = 1.4$. In this paper we investigate the local structure of 2D unsteady disturbances of boundary-layer flow $\varepsilon q(x,y) \exp(-i\omega t) + c.c. + O(|\varepsilon|^2)$, $q = u, v, p, \theta$. The mean flow is assumed to be homogeneous in x-direction in the region under consideration.

To illustrate the influence of wall compliance on the stability of the boundary-layer flow, we consider the simplest law of wall elasticity

$$y_w = -\sigma \, \varepsilon p(x, 0) \exp(-i\omega t) + c.c.$$

9

and suppose that the flow is disturbed by spatially growing TS wave:

$$q_0 = q_0^* (y) \exp (i \alpha_0 x) \qquad (4.1)$$

The functions q_0^* and the complex wavenumber α_0 satisfy the eigenvalue problem for Lin-Lees system with the following wall conditions:

$$u_0^* (0) = \sigma \frac{dU}{dy} (0) p_0^* (0) , \quad v_0^* (0) = i \sigma \omega p_0^* (0) , \quad \theta_0^* (0) = 0$$

In the case of a stiff wall $(\sigma = 0)$ for $R = 1000$, $\omega = 0.05$ we have $\alpha_0 = 0.134 - i\, 0.002$ so boundary layer is unstable. At $\sigma = 10$ the flow becomes stable: $\alpha_0' = 0.116 + i\, 0.004$. This type of TS wave suppression was proposed in [15].

4.2. Cancellation of incoming TS wave by a vibrator

Another way of TS wave suppression was offered in [16]. The general idea of the method consists of the cancellation of the incoming TS wave with the aid of the artificial TS wave generated by a 2D vibrating hump. This cancellation becomes possible because of a special choice of the amplitude and phase of hump oscillations. Here we analytically investigate this method of TS wave suppression.

Simulating the action of an artificial TS wave generator, we assume that a localized part of the plate surface executes the harmonic oscillations in the y-direction with the frequency equal to that of the incoming TS wave:

$$y_w = \varepsilon \, f (x) \exp (-i \omega t) + c.c. \qquad (4.2)$$

The flow disturbance generated by the simultaneous influence of the incoming TS wave (4.1) and the vibration (4.2) takes the following form:

$$q = q_0 + q_v$$

In order to solve the problem for $q_v (x, y)$, it is convenient to make Fourier decomposition:

$$q_v = (2\pi)^{-1} \int f^* q_v^* (y) \exp (ikx) \, dk , \quad f^* (k) = \int f (x) \exp (-ikx) \, dx$$

The normalized Fourier transform q_v^* satisfies the Lin-Lees system and the following wall conditions:

$$u_v^* (0) = -\frac{dU}{dy} (0) , \quad v_v^* (0) = -i \omega , \quad \theta_v^* (0) = 0$$

The form of the artificial TS wave generated by the vibrator is determined by the residue contribution due to the pole of q_v^* at $k = \alpha_0$ (the eigenfunction is assumed to be normalized by the condition $p_0^* (0) = 1$):

$$q_{v0} = f^* (\alpha_0) A \, q_0^* (y) \exp (i \alpha_0 x) , \quad A = \operatorname*{res}_{k = \alpha_0} [i p_v^* (0)]$$

We want the incoming and artificial TS wave to cancel each other downstream the vibrator. Let

$$f = \delta F (x) , \quad \max |F| = 1$$

10

where δ is a complex constant and F is a real function. The condition of mutual cancellation of the two TS waves

$$q_0 + q_{v0} \equiv 0$$

will be satisfied if we assume that

$$\delta = \frac{1}{F^*(\alpha_0) A}$$

For the case of triangular vibrator $F(x) = 1 - |x/l|$, $|x| \leq l$ we have $|\delta| = 43.5$, $\arg \delta = 1.95$ ($R = 1000$, $\omega = 0.05$, $l = 20$).

4.3. Passage of instability wave over a wall of irregular flexibility

Our main object is to study the interaction between TS wave and inhomogeneous flexibility of the wall. The incoming TS wave generates the oscillations of the compliant section

$$y_w = -\sigma F(x)\ \varepsilon p(x,0) \exp(-i\omega t) + c.c. \tag{4.3}$$

where $F(x)$ is longitudinal distribution of the wall flexibility. In contrast to the vibrator problem, in this case the form of surface oscillations $f(x)$ is unknown function to be determined from the solution of the whole problem.

The connection between pressure disturbance and the vibration form can be obtained from the solution of the vibrator problem [14]:

$$p(x,0) = \exp(i\alpha_0 x) + I[f] \tag{4.4}$$

$$I[f] = (2\pi)^{-1} \int p_v^*(0)\, dk \int f(\xi) \exp[ik(x-\xi)]\, d\xi$$

Using the equalities (4.2) -(4.4) , we obtain the basic integral equation:

$$f = -\sigma F\ \{\exp(i\alpha_0 x) + I[f]\} \tag{4.5}$$

We introduce a quantitative TS wave modification characteristic - the complex passage coefficient K_p:

$$K_p = \frac{q_0 + q_{v0}}{q_0} = 1 + f^*(\alpha_0) A \tag{4.6}$$

- the ratio between the complex amplitudes of the passed and incoming TS wave.

At first, let us consider the limiting case $\sigma \to 0$. The equality (4.6) takes the form

$$K_p = 1 - \sigma A \int F(x)\, dx + O(\sigma^2) \tag{4.7}$$

This result is obtained from the considerations based on receptivity phenomenon. The same result may be obtained from the investigation of TS wave propagation over the long flexible section $F_0(x) \equiv 1$, $0 \leq x \leq L$, $L \gg 1$. Over this section the disturbance can be regarded as TS wave over the wall of small uniform flexibility (except the neighbourhoods of the joins $x = 0$ and $x = L$). Based on stability phenomenon, these considerations give the following equation for the passage coefficient:

$$K_p = \frac{\exp(i\alpha_0' L)}{\exp(i\alpha_0 L)} = 1 + i\left(\alpha_0' - \alpha_0\right) L + O(\sigma^2) \tag{4.8}$$

11

The equation (4.8) coincides with (4.7) since the perturbation method leads to the equality

$$\alpha_0' = \alpha_0 + i\sigma A + O\left(\sigma^2\right)$$

Thus, the quantitative TS wave attenuation characteristics can be obtained both by studying the stabilizing effect of the wall elasticity and by analyzing the formation of the secondary TS wave generated by the wall vibration.

Now consider the general case $\sigma = O\left(1\right)$. This investigation is based on the numerical solution of the integral equation (4.5). The results of calculations for the magnitude $|K_p|$ of the passage coefficient are shown in Figure 19. The calculations are made for flexibility distribution

$$F\left(x\right) \equiv 1 \,, \qquad\qquad |x| \leq l$$

$$F\left(x\right) = 1 - 2\left(\frac{|x| - l}{a}\right)^2 \,, \qquad l \leq |x| \leq l + \frac{a}{2} \qquad\qquad (4.9)$$

$$F\left(x\right) = 2\left(\frac{|x| - l}{a} - 1\right)^2 \,, \quad l + \frac{a}{2} \leq |x| \leq l + a$$

with $l = 10$, $a = 4$. The outlined results show a good agreement between linear theory (4.7) and exact solution (4.6) up to $\sigma = 1$. The value $|K_p|$ has minimum in the vicinity of $\sigma = 10$. At $\sigma = 20$ this flexible section loses the capacity of TS wave suppressing.

The process of TS wave suppression by the compliant section (4.9) is shown in Figure 20 for $R = 1000$, $\omega = 0.05$, $\sigma = 10$ and $l = 100$, $a = 4$. In the region over the compliant section the disturbance is closely approximated by the relaxing TS wave over the wall of uniform flexibility $\sigma = 10$, with the complex amplitude at $x = -l$ being not equal to that of the incoming TS wave.

Consider the propagation of TS wave over a join between semi-infinite rigid and compliant wall: $F\left(x\right) \to 0$ as $x \to -\infty$ and $F\left(x\right) \to 1$ as $x \to +\infty$. We introduce the complex transformation coefficient K_{tf} - the ratio between the complex amplitudes of the incoming and passed TS wave. This value may be determined from the equation

$$K_{tf} = -\frac{1}{f^*\left(\alpha_0\right) A}$$

using the solution of the following problem:

$$f = -\sigma F \, I\left[f\right] \,, \quad f \to -\sigma \exp\left(i\alpha_0' x\right) \text{ as } x \to +\infty$$

Contrary to the case of passage coefficient, the value of transformation coefficient depends on the location of the coordinate origin.

4.4. Interaction of other eigenmodes with wall irregularity

Up to this point we have studied the scattering of TS wave into TS wave by wall inhomogeneity. Scattering of TS wave into other discrete or continuous eigenmodes may be investigated in a similar way: the amplitudes of generated eigenmodes can be determined using Cauchy's integral theorem for calculation the integral $I\left[f\right]$. Moreover, TS wave may be generated via scattering of other eigenmodes (discrete or continuous) by the

12

wall irregularity. This process is characterized by the complex transmutation coefficient K_{tm}(the ratio between complex amplitudes of incoming and scattered mode). This coefficient may be determined from the solution of the equation (4.5) with α_0 replaced by α (the wavenumber of new eigenmode).

In Figure 21 the process of transmutation of stable discrete eigenmode into TS wave is shown for the same parameters as in the above case. The wavenumber of incoming wave $\alpha_1 = 0.092 + i0.061$. Figure 22 illustrates the scattering of sound propagating downstream (the mode from continuous spectrum), into TS wave for the same parameters and $\alpha_s = 0.022 + i\,2\cdot 10^{-7}$.

In our investigation we have demonstrated that the stability and receptivity phenomenon in inhomogeneous flow have a common feature: the stability is the process of scattering of TS wave into TS wave, while the receptivity describes the scattering of continuous mode into TS wave.

References

[1] Bushnell, D. (1994) Viscouse drag reduction in aeronautics, *ICAS'94 Proceedings, Anaheim, USA, September 18-23, 1993*

[2] Breuer, K.S. & Landahl, M.T.(1990) The evolution of localized disturbances in a laminar boundary layer. Part 2. Strong disturbances, *J. Fluid Mech.*, **220**, 595-621.

[3] Butler K. M.O.& Farrel B.F. (1992) Three-dimensional optimal perturbations in viscous shear flows, *Phys. Fluids, A*, **4**, 1637-1650.

[4] Goldstein, M.E., Leib,S.I.& Cowley, S.J. (1992) Distortion of a flat-plate boundary layer by free-stream vorticity normal to the plate, *J. Fluid Mech.*, **237**, 231-260.

[5] Townsend, A.A. (1970) Structure of turbulent shear flows, 2nd edu. Cambridge University Press.

[6] Wygnansky, I., Champague, F. & Marasli, B. (1986) On the large-scale structures in two-dimensional, small deficit, turbulent wakes, *J. Fluid Mech.*, **168**, 31-71.

[7] Grek, G.R.,Kozlov, V.V. & Ramazanov, M.P. (1991) Laminar-turbulent transition in a flow with enhanced turbulence level, *Sib. fiz.-tech Jurnal*, issue 6, 106.

[8] Hunt, I.C.R. & Carruthers D.J. (1990) Rapid distortion theory and "problems"of turbulence, *J. Fluid Mech.*, **212**, 497-532.

[9] Stewart, P.A. & Smith, F.T. (1992) Three-dimensional nonlinear flow-up from a nearly planar initial disturbances in boundary-layer transition, *J. Fluid Mech.*, **224**, 79-100.

[10] Walton, A.G. & Smith, F.T. (1992) Properties of strongly non-linear vortex/Tollmien-Schlichting-wave interactions, *J. Fluid Mech.*,**244**, 649-677.

[11] Bertolotti, F.P., Herbert, T. & Spalart, P.R. (1992) Linear and nonlinear stability of the Blasius boundary layer, *J. Fluid Mech.*,**242**,441-474.

[12] Herbert, T. (1991) Boundary-layer transition - analysis and prediction revised, *AIAA paper,* No 91-0737.

[13] Kachanov, Yu.S. & Levchenko, V.Ya. (1984) The resonant interaction of disturbances at laminar-turbulent transition of a boundary layer, *J. Fluid Mech.,* **148**, 43-74.

[14] Manuilovich, S.V. (1988) On the receptivity of subsonic flow to oscillating effects localized at the base of the boundary layer, *Izv. Akad. Nauk SSSR, Mekh. Zhidk. Gaza,* No. 4, 63-69.

[15] Kramer, M.O. (1957) Boundary layer stabilization by distributed damping, *J. Aeron. Sci.* **24**, 459-460.

[16] Milling, R.W. (1981) Tollmien-Schlichting wave cancellation, *Phys.Fluids* **24**, No. 5, 979-981.

[17] Manuilovich, S.V. (1992) Passage of an instability wave through a channel section of variable width *Izv. Ros. Akad. Nauk, Mekh. Zhidk. Gaza,* No. 2, 34-41.

[18] Terent'ev, E.D. A linear problem of a vibration in a boundary layer on a partially elastic surface *International Workshop on Advances in Analytical Methods in Aerodynamics,* Miedzyzdroje, Poland, 12-14 July 1993.

[19] Davies, C. & Carpenter, P.W. Tollmien-Schlichting waves propagating over the join between a rigid and compliant wall, *2nd European Fluid Mechanics Conference.* Warsaw, Poland, 20-24 Sept. 1994.

Table 1

U m/sec	U$'$/U	U$'$/U (f>5 hz)
5	0.25%	0.06%
10	0.25%	0.04%
15-65	------	0.03%

Table 2

No	D[mm]	Xo[mm]	U_o / U_∞	L[mm]
I	0.8	455	0.045	6.2
II	0.8	225	0.059	4.8
III	0.8	100	0.076	3.7
IV	1.6	125	0.084	6.7

Wind tunnel T-36i

FIGURE 1

Spectrum U = 5 m/sec
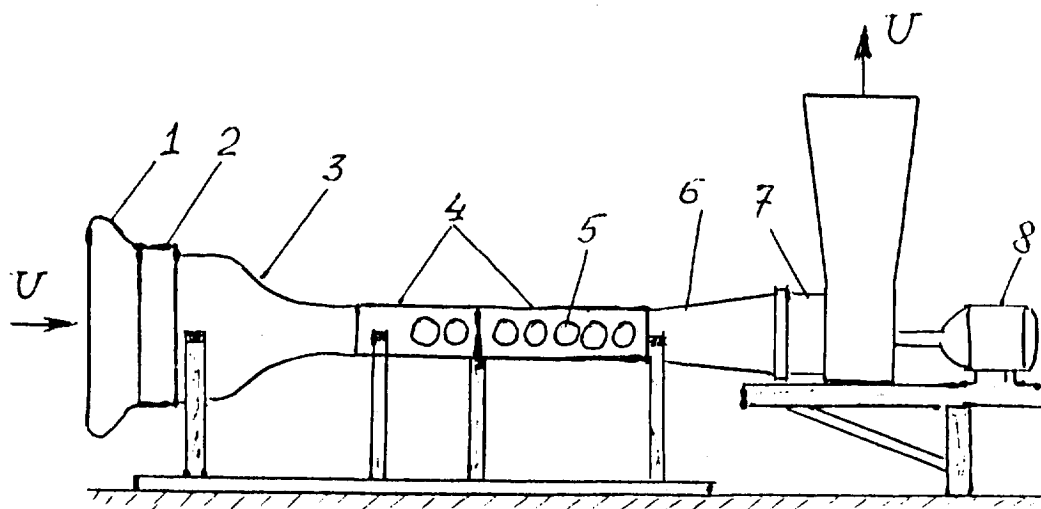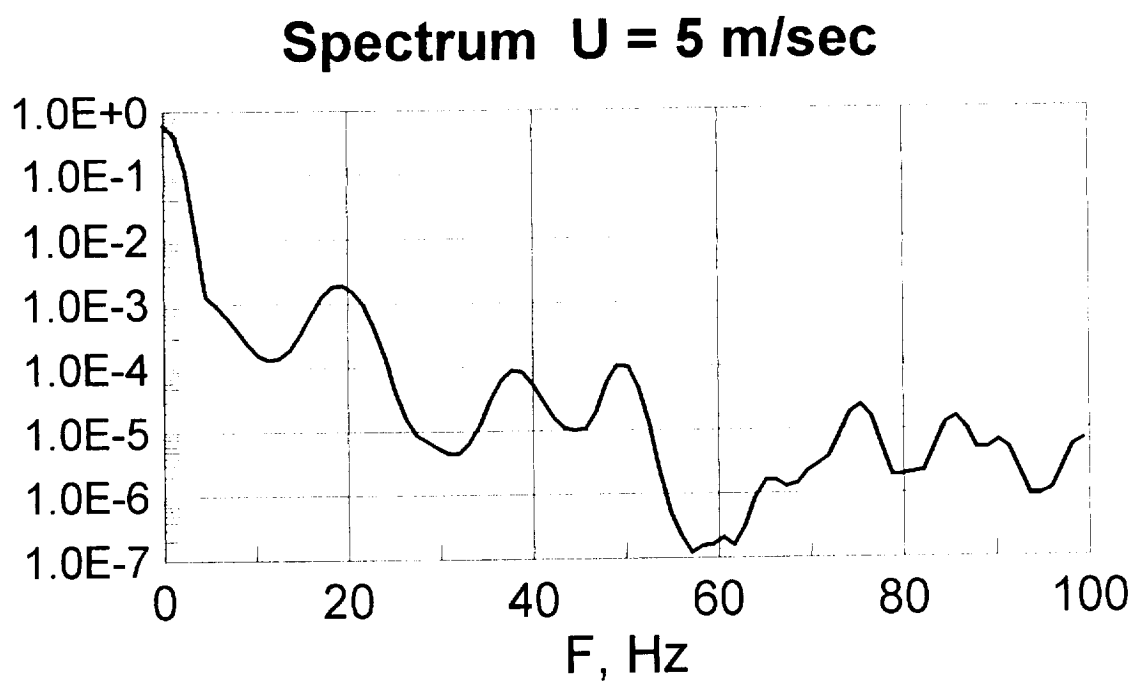
FIGURE 2

FLOW CONFIGURATION

a) Wake measurements
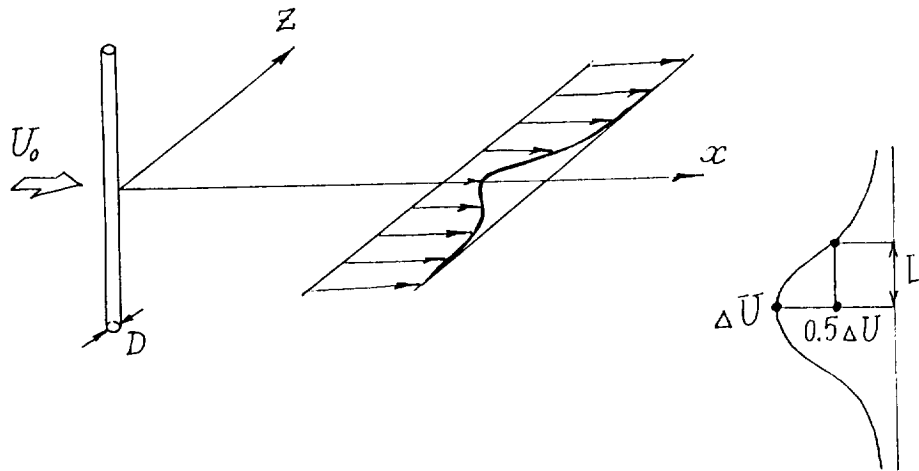
b) Wake - boundary layer interaction
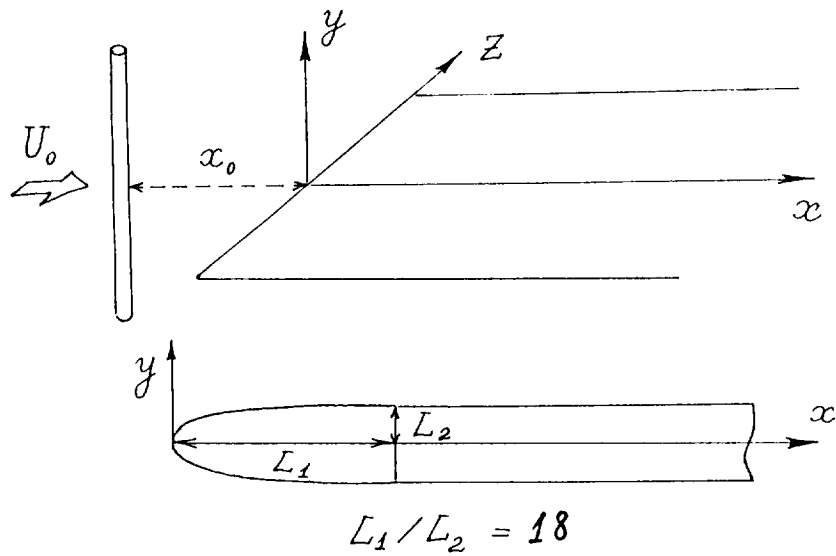
$$L_1 / L_2 = 18$$

FIGURE 3

MEAN FLOW IN LAMINAR WAKE

$$D = 0.1 \ mm , \quad U_0 = 5 \ m/s , \quad R = U_0 D / \nu = 34.5$$
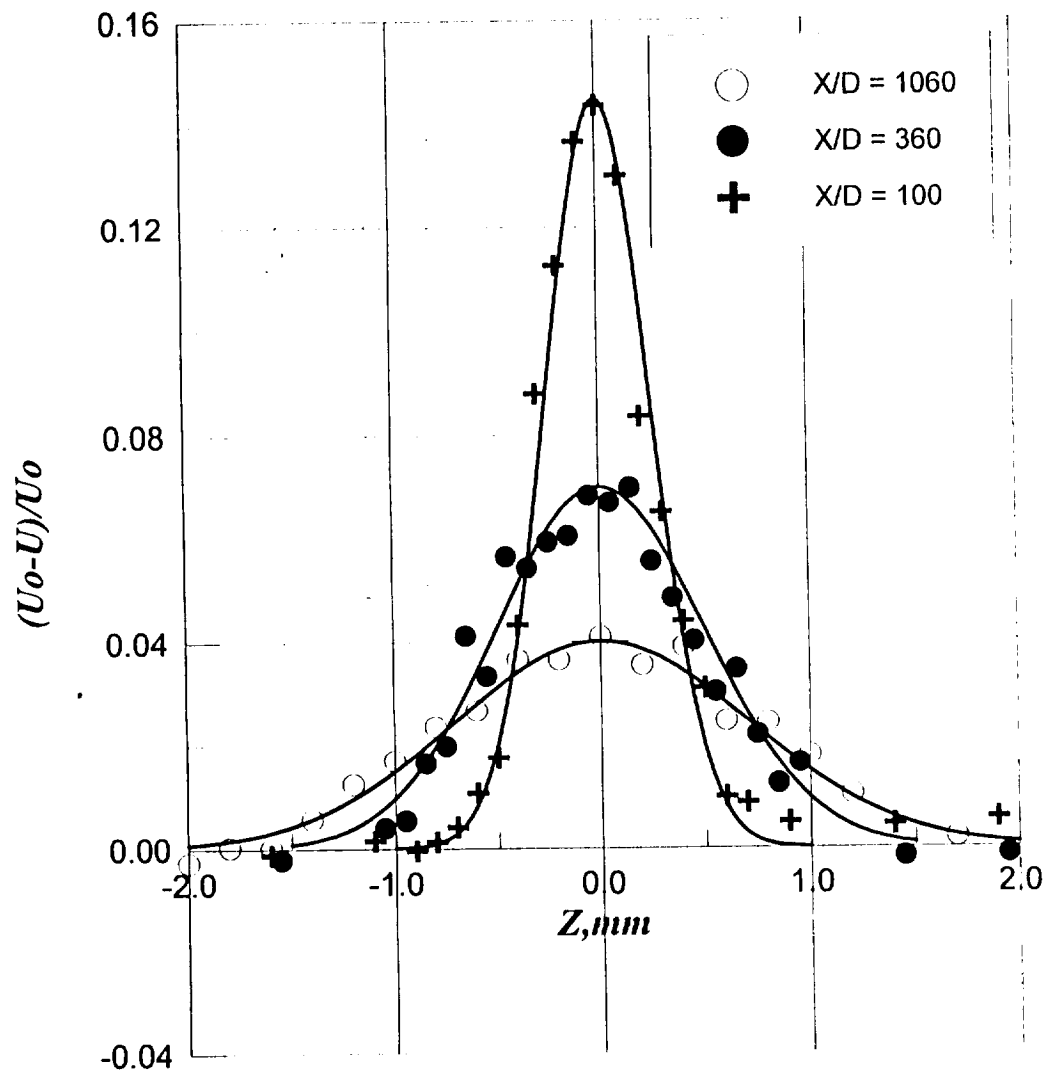
FIGURE 4

MEAN FLOW IN LAMINAR WAKE II
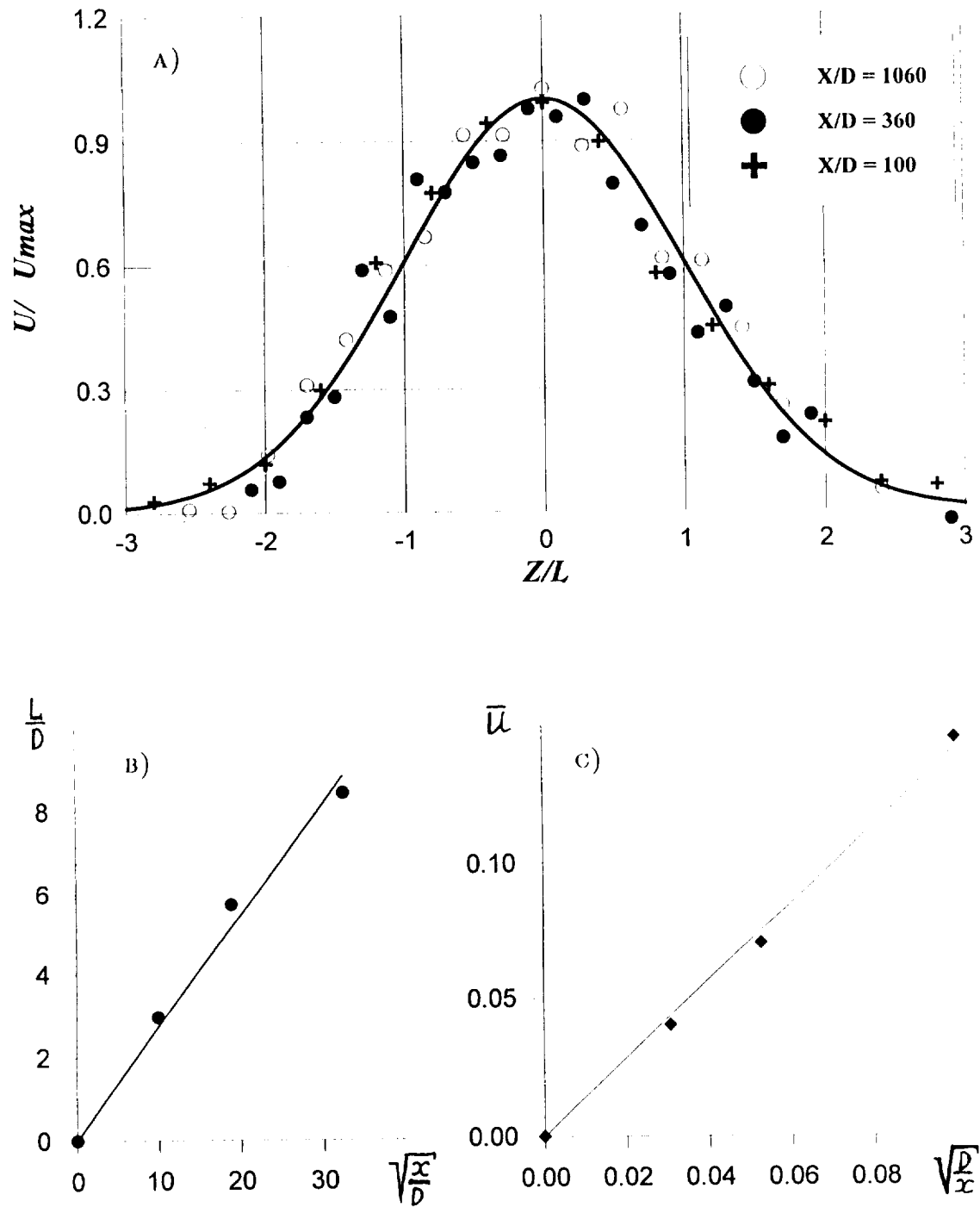
FIGURE 5

PULSATIONS IN LAMINAR WAKE

Unfiltered Pulsations
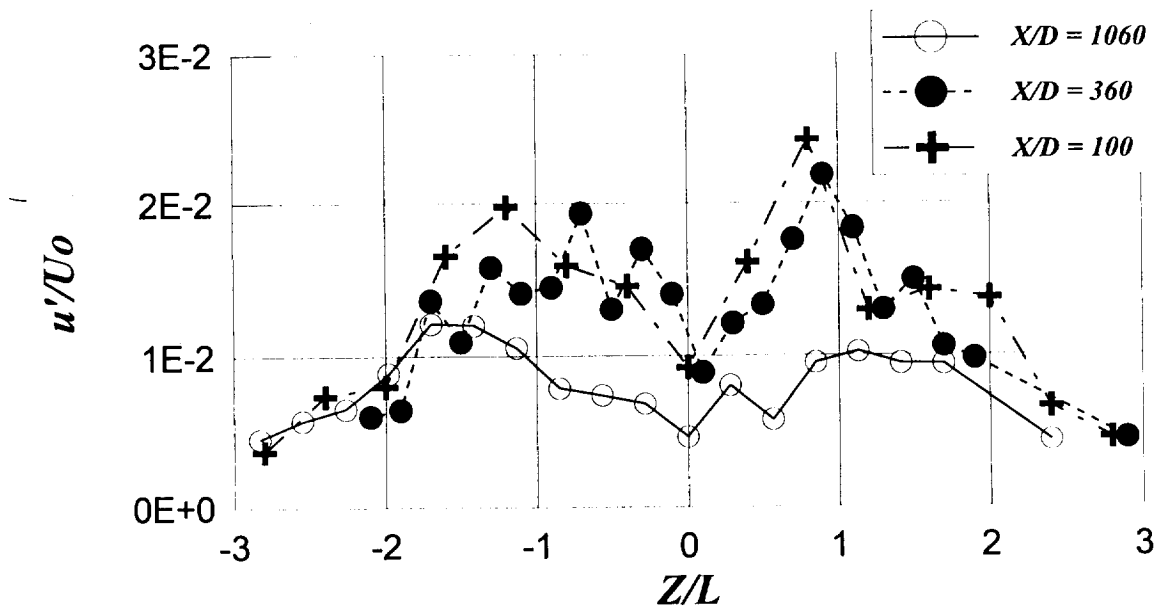
Filtered Pulsations f > 5 Hz
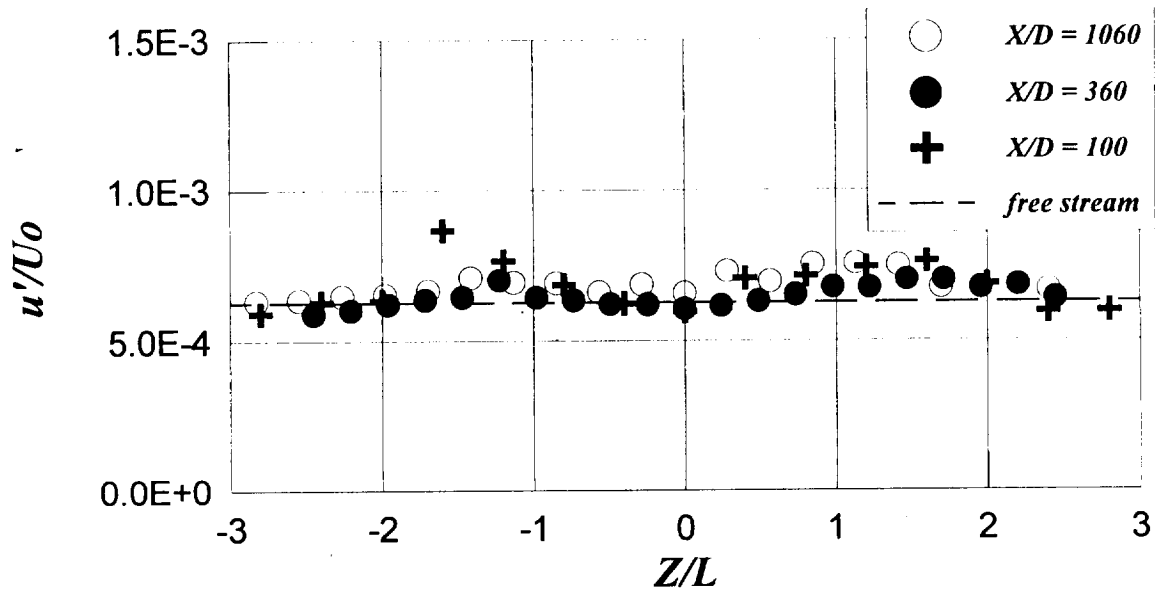
FIGURE 6

Turbulent wake

Uo = 10 m/sec, D=1.6 mm, Rd=1100, X/D=220
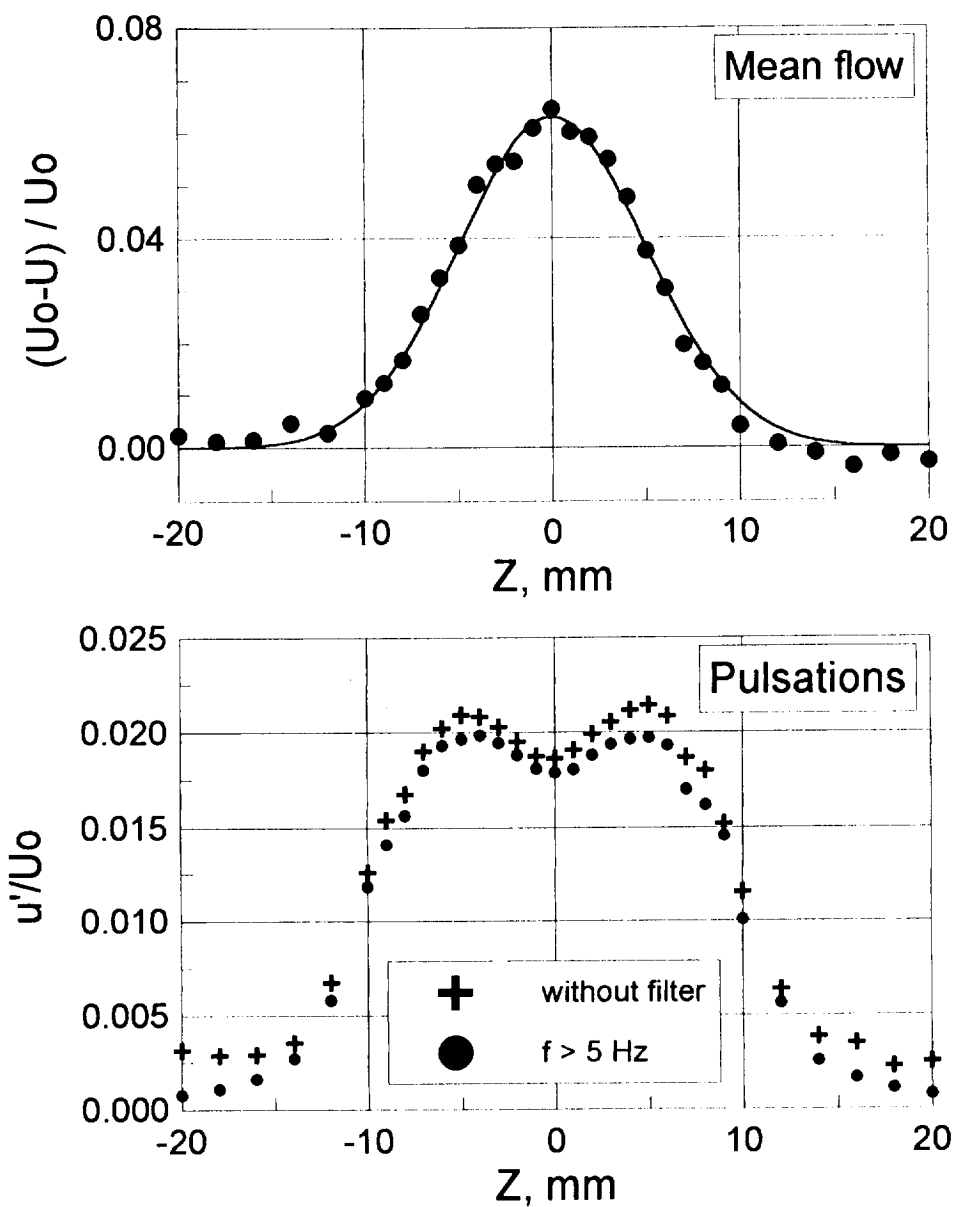
FIGURE 7

Spectrum of pulsations in turbulent wake
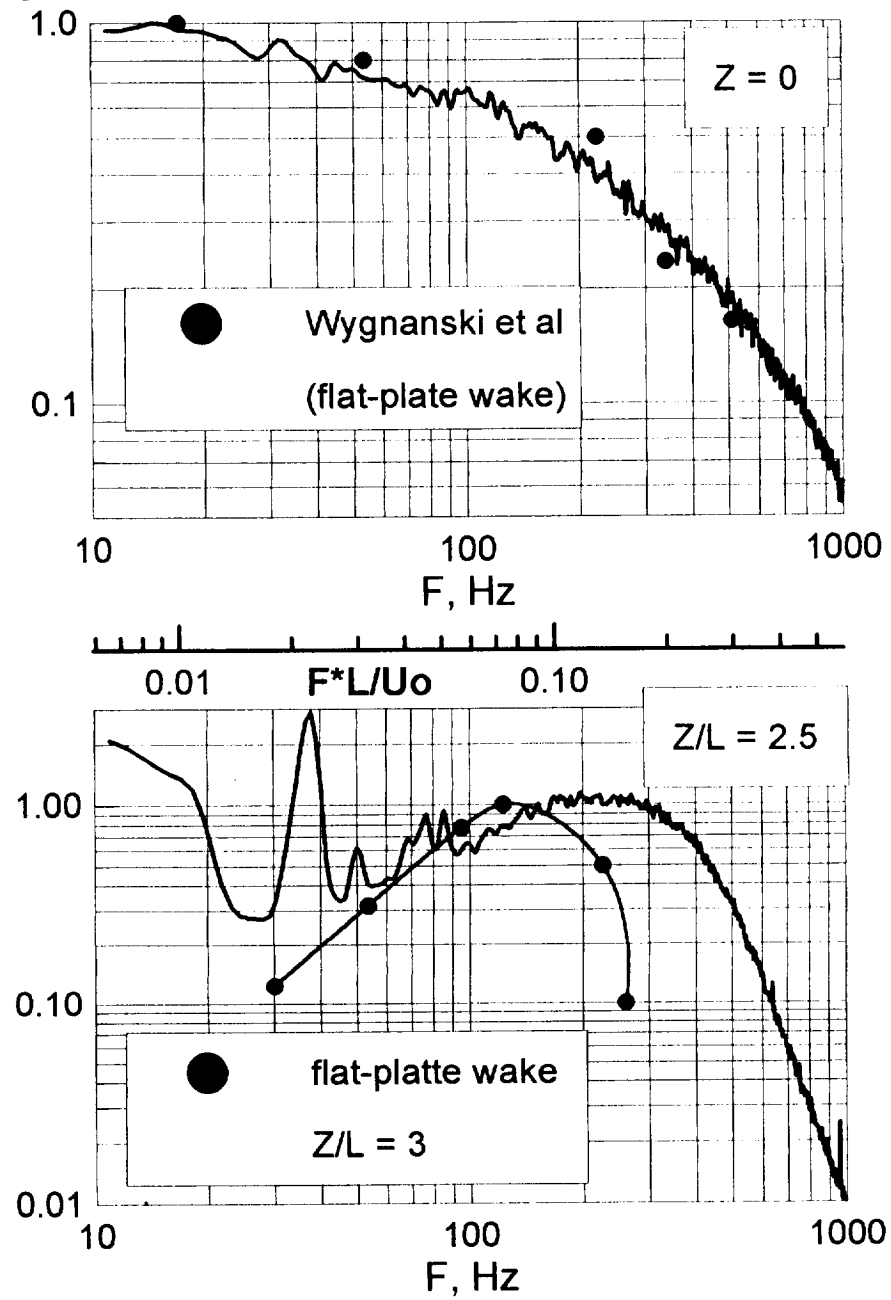
FIGURE 8

Wake - boundary layer interaction

Mean flow

Pulsations (f > 5 Hz)

(see table 2)

●	I
□	II
+	III
△	IV
▲	no wire
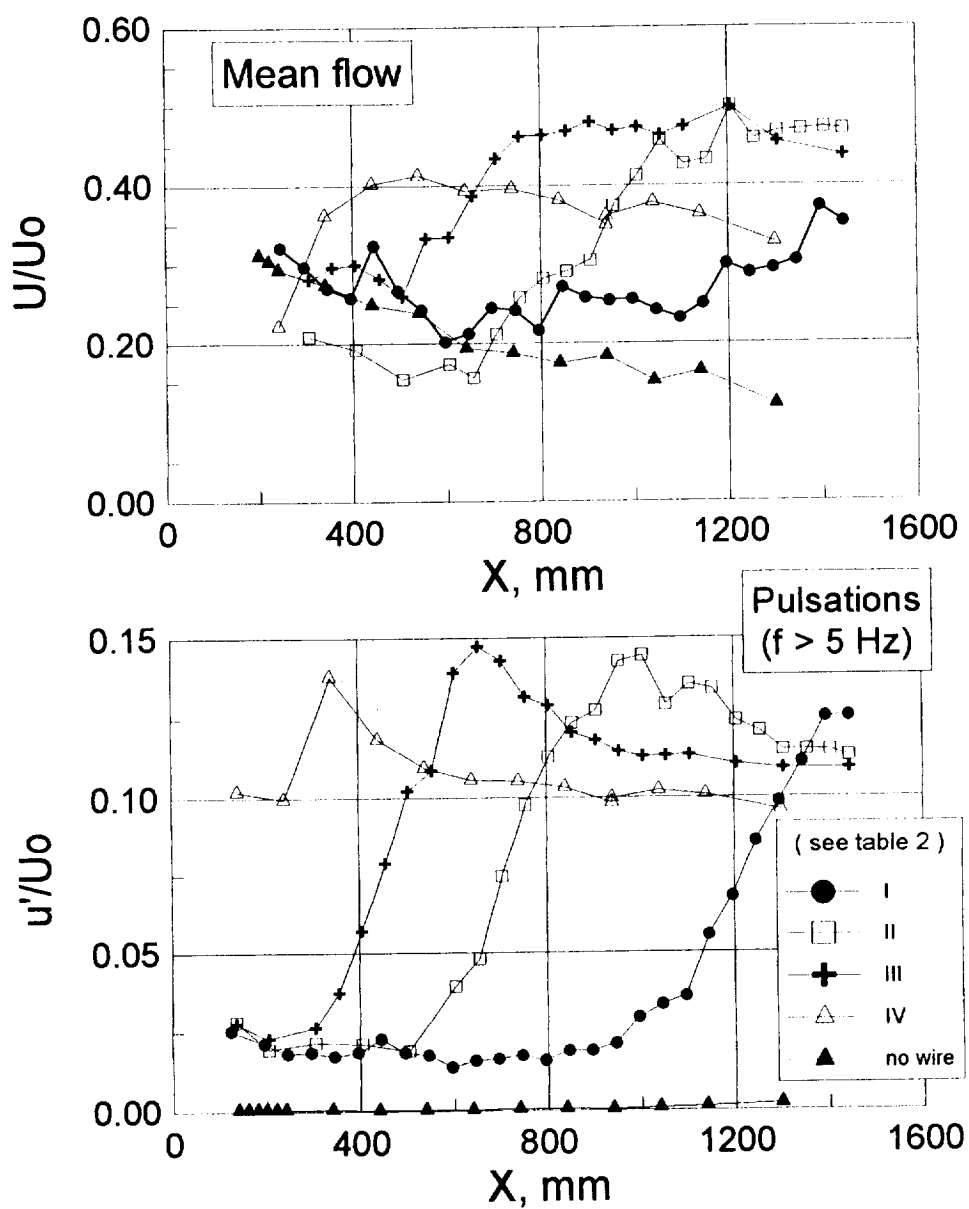
FIGURE 9

Wake-boundary layer interaction

● outer flow ◇ boundary layer

Mean flow

X = 200 mm

X = 350 mm

X = 525 mm

X = 670 mm

X = 850 mm

Z, mm

Pulsations

X = 200 mm

X = 350 mm

X = 525 mm

X = 670 mm

X = 850 mm

Z, mm
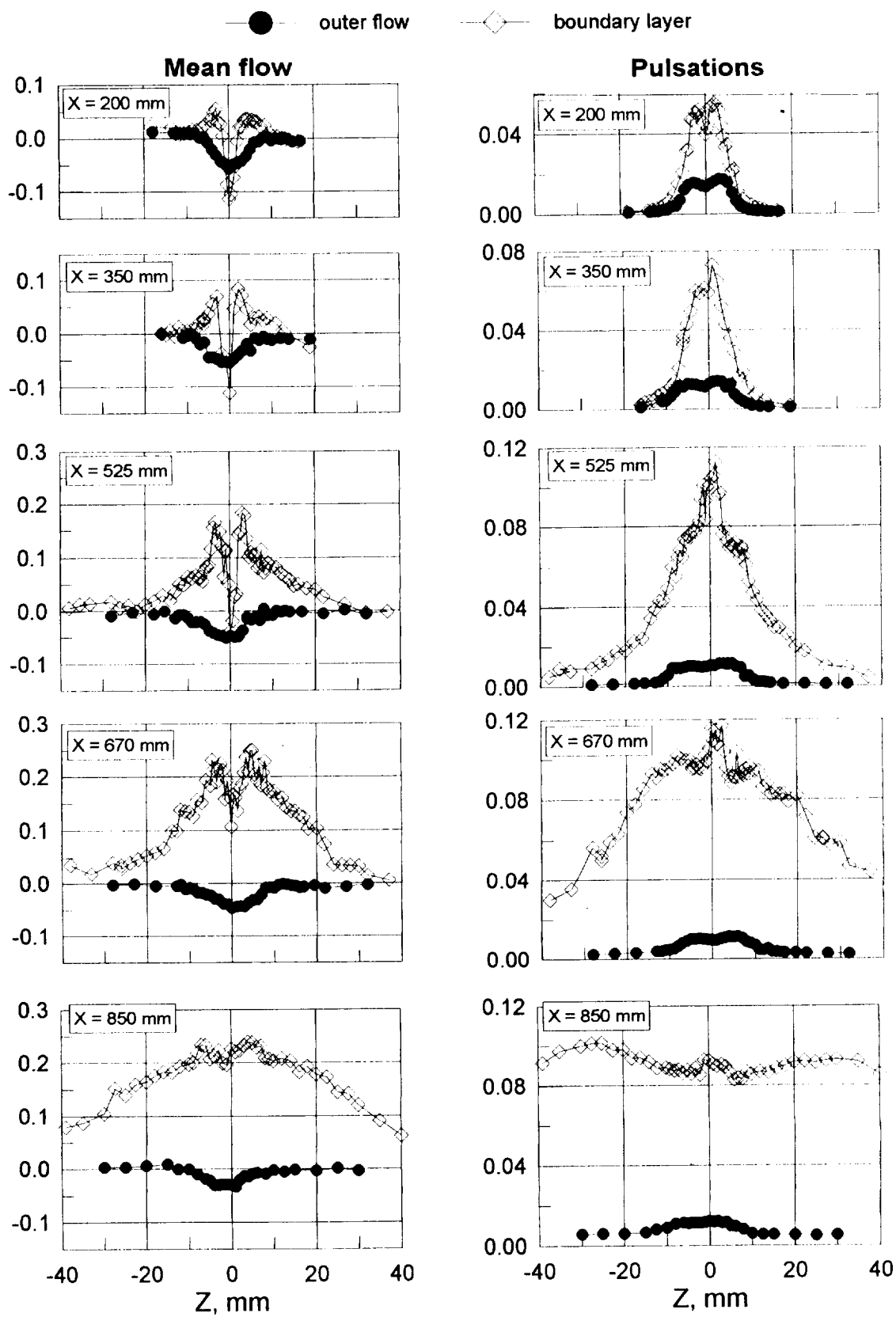
FIGURE 10

Velocity and pulsations profiles
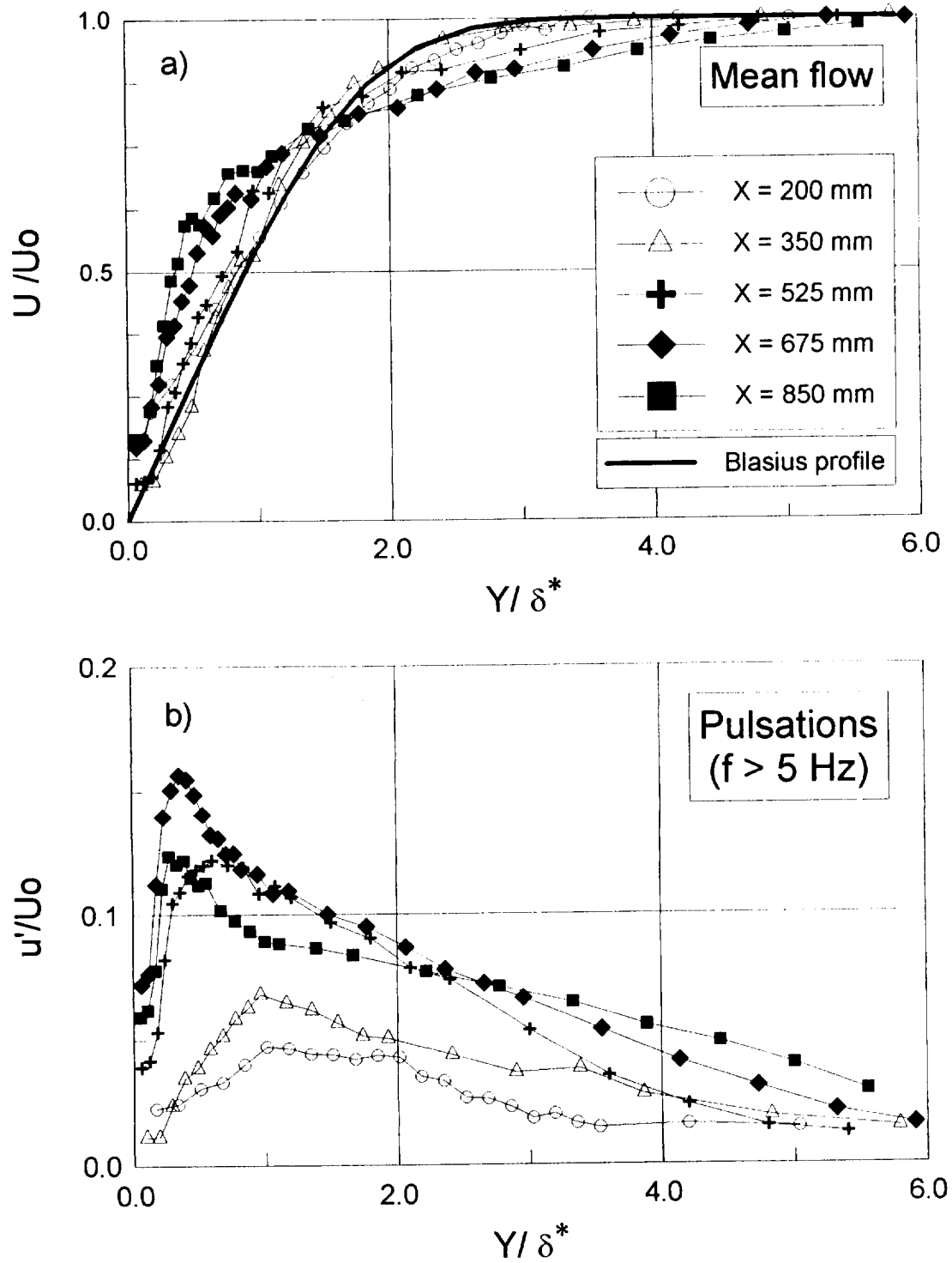
FIGURE 11

Spectra at the centreline
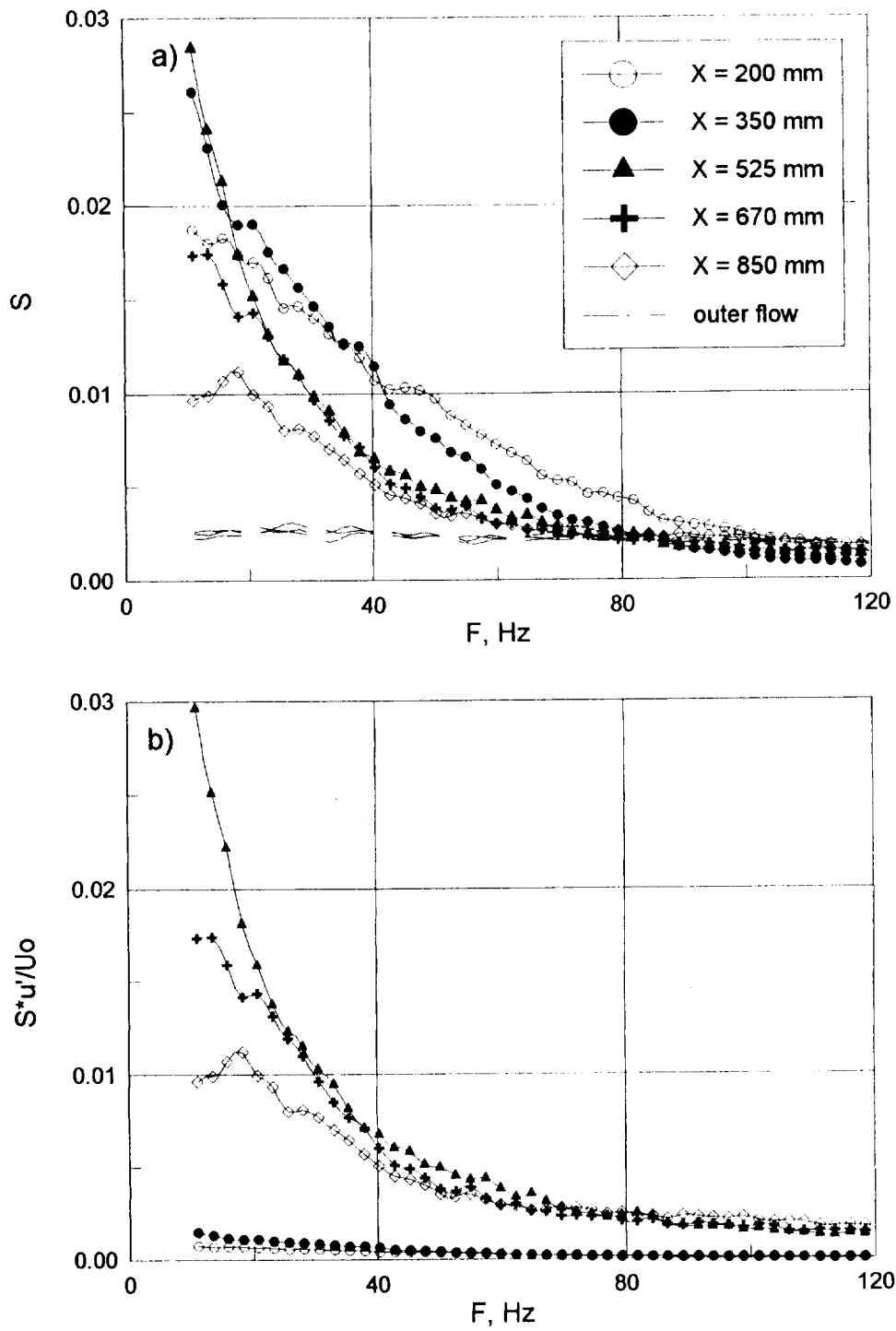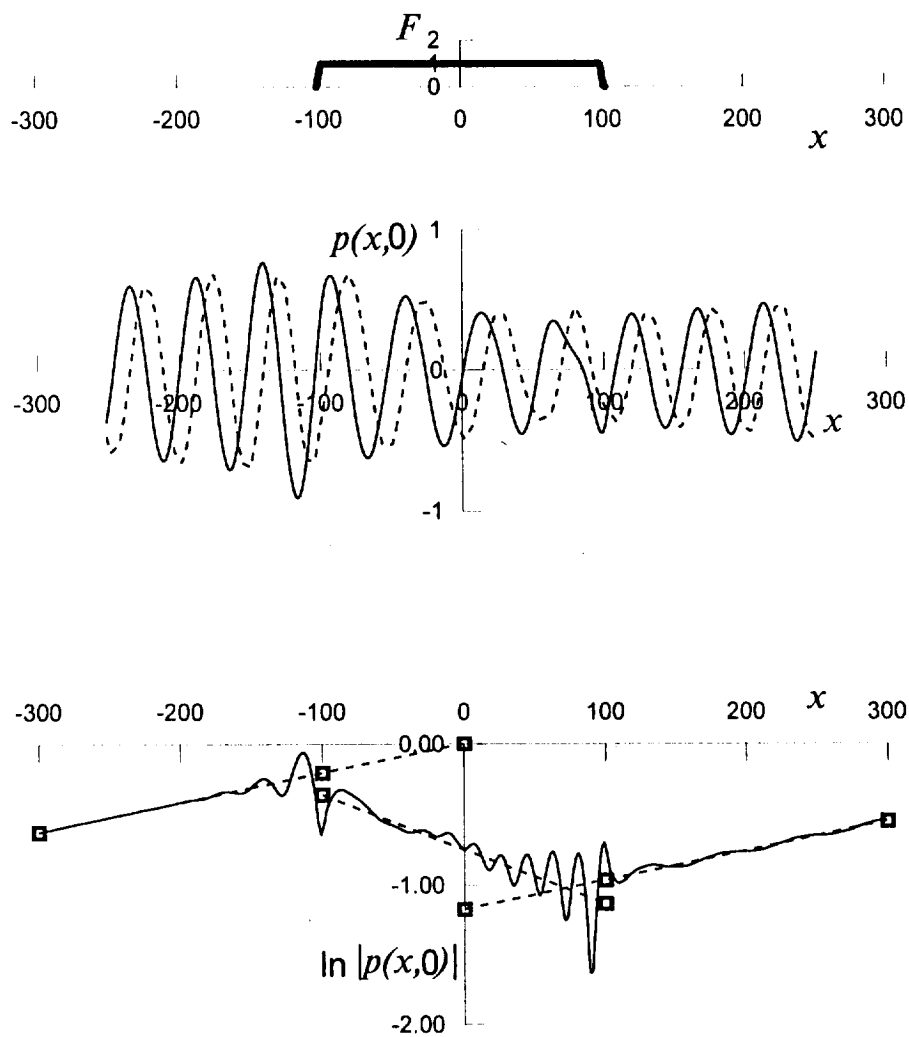

FIGURE 12
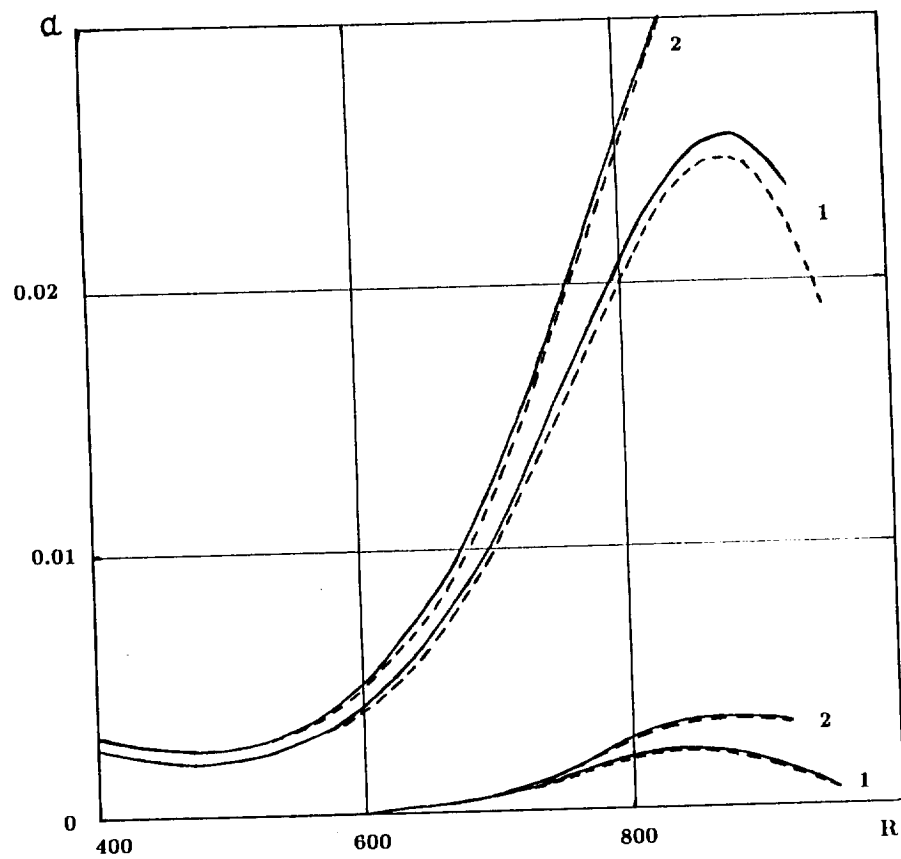
FIGURE 13
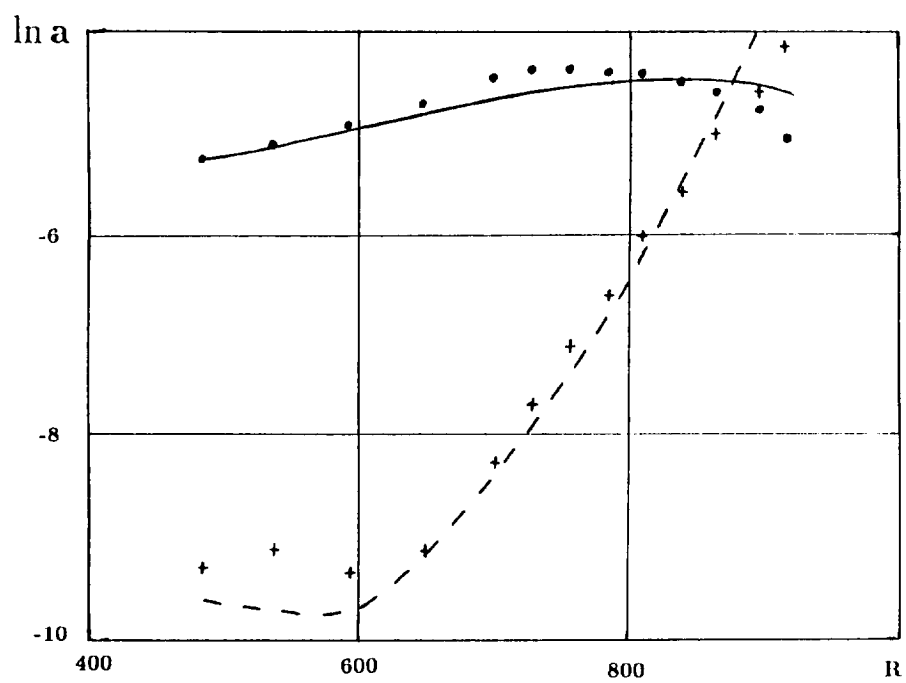
FIGURE 14
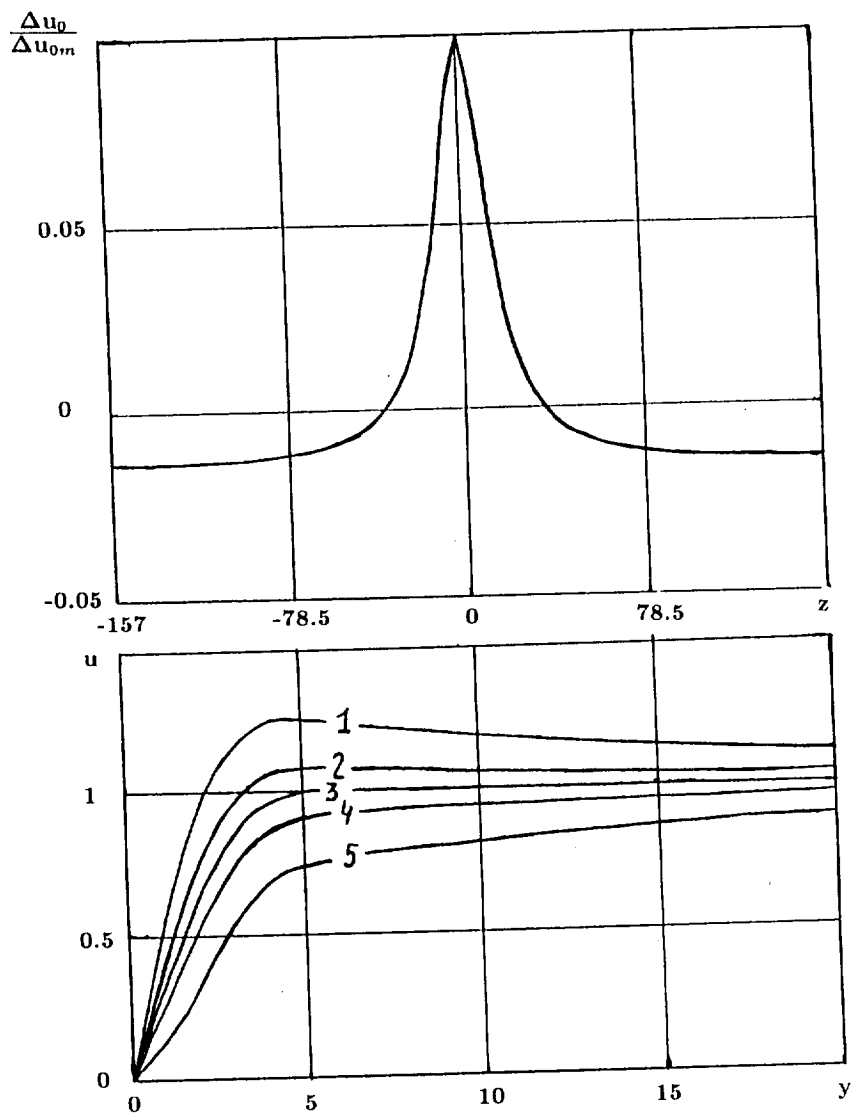
FIGURE 15
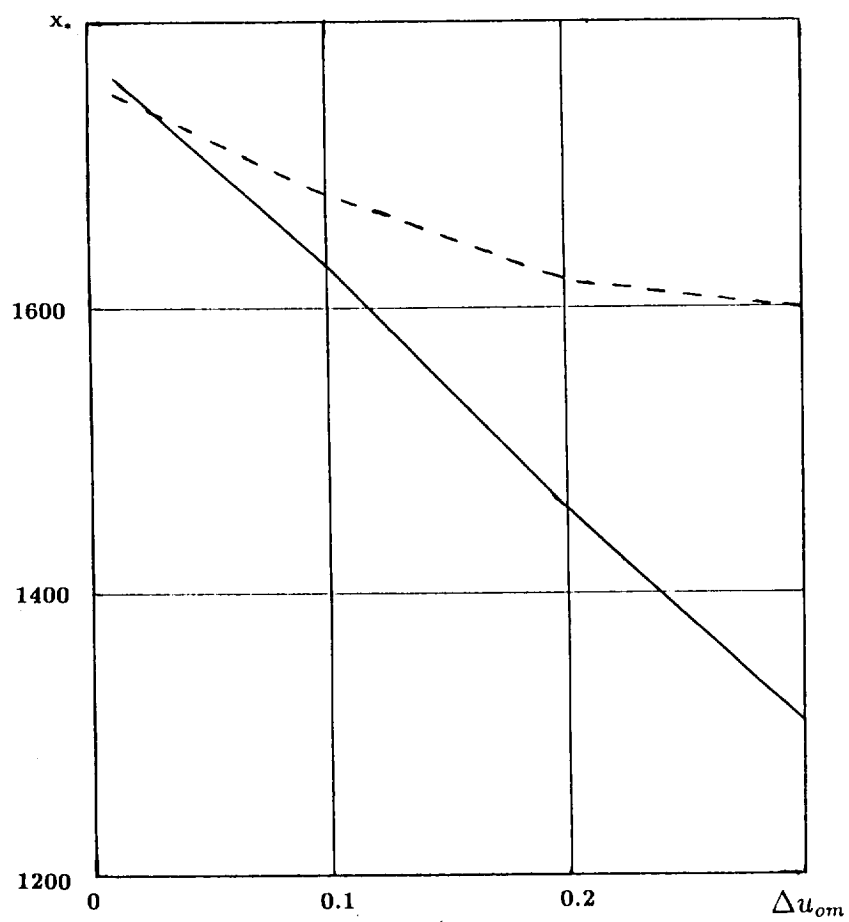
FIGURE 16
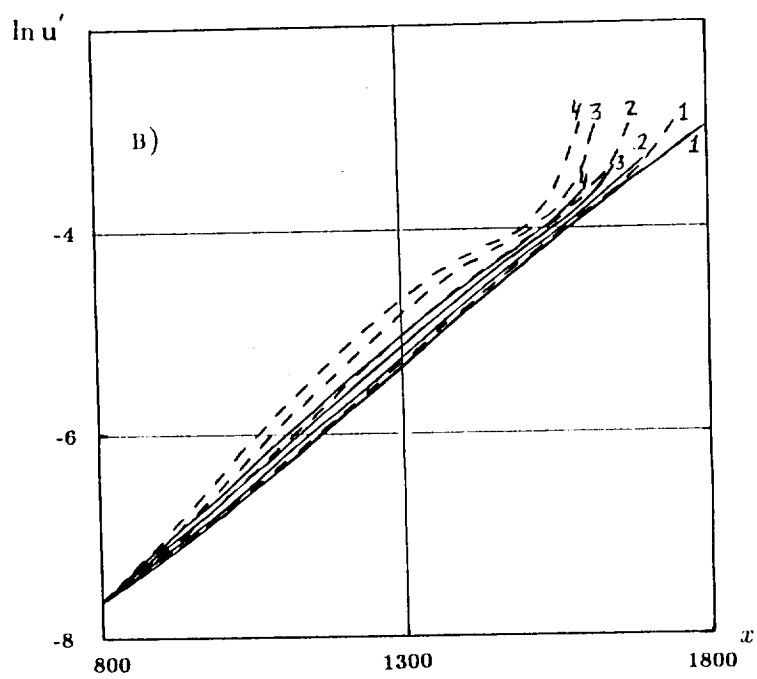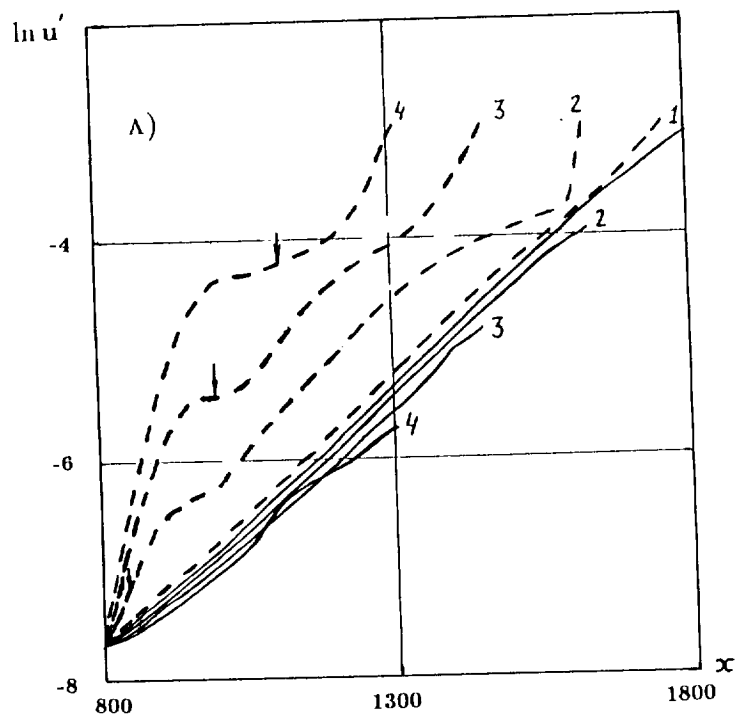
FIGURE 17
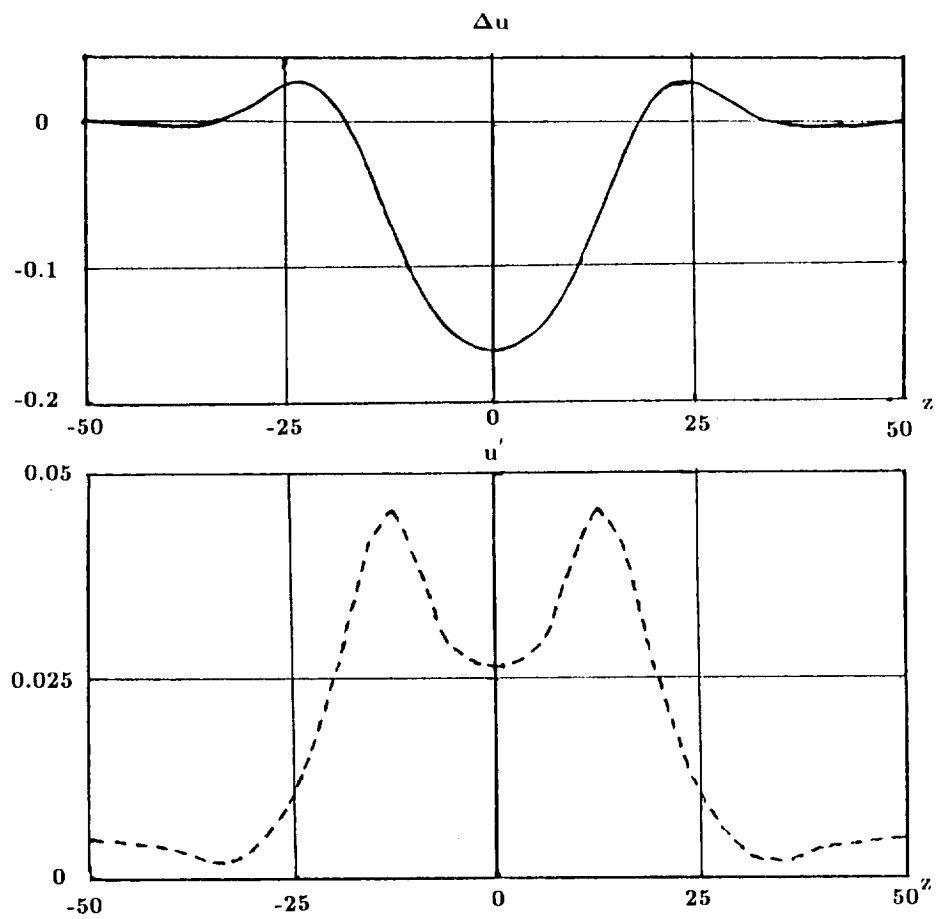
FIGURE 18
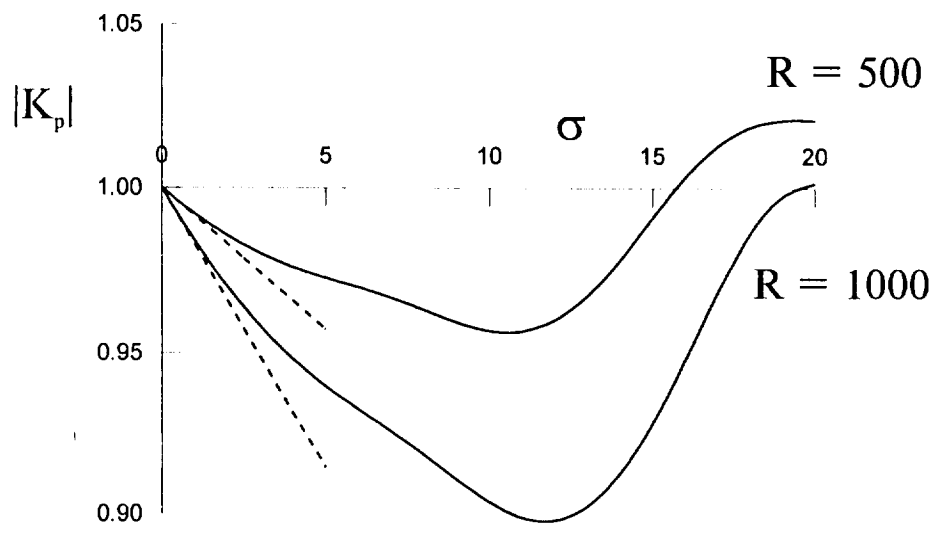
FIGURE 19

FIGURE 20

FIGURE 21

FIGURE 22